



PCCP

**'Reverse' Hofmeister effects on the sol-gel transition rates
for an α -helical peptide-PEG bioconjugate**

Journal:	<i>Physical Chemistry Chemical Physics</i>
Manuscript ID	CP-ART-05-2018-003316.R1
Article Type:	Paper
Date Submitted by the Author:	07-Jul-2018
Complete List of Authors:	O'Neill, Sean; The City College of New York, Department of Chemical Engineering Kanthe, Ankit; The City College of New York, Department of Chemical Engineering Weber, Jacob; The City College of New York, Department of Chemical Engineering Tu, Raymond; The City College of New York, Chemical Engineering

SCHOLARONE™
Manuscripts



Journal Name

ARTICLE

'Reverse' Hofmeister effects on the sol-gel transition rates for an α -helical peptide-PEG bioconjugate

Received 00th January 20xx,
Accepted 00th January 20xx

Sean C. O'Neill,^a Ankit D. Kanthe,^a Jacob A. Weber^a and Raymond S. Tu^{*a}

DOI: 10.1039/x0xx00000x

www.rsc.org/

We examine the dynamics of the sol-gel transition for end-functionalized linear- and 4-arm-peptides bioconjugated to poly-ethylene glycol (PEG) in aqueous environments with increasingly chaotropic ($\text{Cl}^- < \text{Br}^- < \text{I}^-$) anions. A 23-amino acid peptide sequence is rationally designed to self-assemble upon folding into the ordered α -helical conformation due to the hydrophobic effect. We use Attenuated Total Reflection - Fourier Transform Infrared Spectroscopy (ATR-FTIR) to quantify the ensemble average reversible secondary structure transitions as a function of electrolyte concentration and specific ion effects along the Hofmeister series. Subsequently, microrheology is used to quantify the kinetics of the gelation process, as it relates to folding and specific ion interactions. Our key findings were non-intuitive. We observe the faster evolution of the gel transitions in systems with more chaotropic anions. For our peptides in aqueous solution, "water-structuring" ions yield faster assembly behavior with a viscoelastic exponent, n , closer to unity representing self-assemblies that are Rouse-like. In contrast, ions that are "water-breaking" resulted in smaller viscoelastic exponents where self-assembly dynamics result in a viscoelastic exponent that suggests polymer entanglements.

Introduction

Numerous protein-protein bridging interactions are mediated by ion interactions in natural systems that are essential for function in living organisms. These effects have been known for decades¹⁻³. For example, von Hippel and Schleich studied the effects of increasing chloride ion concentrations that results in decreasing melting temperatures for the collagen triple helix⁴. In another collagen study, the folding 'pathways' for α , β and γ collagen subunits into triple helices can be related to ions in the Hofmeister series. In these studies, kosmotropic or "water-structuring" sulfate ions have been shown to increase stability of the triple helix while promoting faster folding kinetics. Kosmotropic ions have small radii with lower hydration entropies providing a well-hydrated solute that can effectively "salt-out" proteins and lower their solubility. In contrast, interaction with chaotropic or "water-breaking" thiocyanate ions can promote a "salting-in" effect. These chaotropic ions are typically responsible for denaturing proteins. Chaotropic ions have large radii that are poorly-hydrating and lower the interfacial surface tension at the hydrophobic regions of proteins. As a result, the chaotropic ions have a higher local concentration near hydrophobic

peptide interfaces resulting in an increase in solubility. Mid-kosmotropic/chaotropic ions are neither water "breakers" nor "structurers", and ions such as chloride and acetate were shown to have minimal influence on collagen folding⁵⁻⁸. A fundamental understanding of the Hofmeister effect can allow one to rationally design bioconjugates that will respond to specific ionic environmental cues⁹.

Our model system examines specific ion effects on a rationally designed amphiphilic peptide, investigating the α -helical stability as well as the dynamics of self-assembly and gelation. The electrolytes used in this work are monovalent anions in the Hofmeister series, including chloride, bromide and iodide species. The ions play a dual role in the folding of the peptide into helices. First, the ion promotes helical stability through the non-specific charge screening, and, second, the specific ion effects will promote salting-in and salting-out near hydrophobic interfaces¹⁰⁻¹². Typically, these anions become increasingly destabilizing or chaotropic for larger radii as they salt-in, breaking water structure and facilitating peptide-water interactions. The chaotropic ions are known to increase the denaturation of both α -helices and β -sheets. The kosmotropic ions with smaller radii have the opposite effect, typically enhancing peptide folding and self-assembly due to increased peptide-peptide interactions and decreased solubility. Thermodynamically, kosmotropes have large positive activation energies and unfavorable water dissociation entropies, while the converse is true for chaotropes¹³⁻¹⁵.

The design of model peptide-polymer bioconjugates has been described by previous studies to investigate ion-peptide interactions on self-assembly and gelation dynamics. The

^a Department of Chemical Engineering, The City College of City University of New York, 140th Street and Convent Avenue, Steinman Hall T313, New York, New York 10031 USA. E-mail: tu@ccny.cuny.edu

† Footnotes relating to the title and/or authors should appear here.

Electronic Supplementary Information (ESI) available: [details of any supplementary information available should be included here]. See DOI: 10.1039/x0xx00000x

sequence, EKAEKLLKLLKAWEKLEKAEK has been shown to form tetrameric parallel and anti-parallel helical self-assemblies driven by the hydrophobic coiled-coil assembly. Exposure of the peptide to a basic environment or a high concentration electrolyte solution promotes α -helical peptide secondary structure and results in the spatial separation of the hydrophobic and hydrophilic faces of the helix^{16–19}. On folding and self-assembly, we can use particle tracking passive microrheology to examine the gelation dynamics^{20,21}. We compare the ion-specific gelation rates of linear peptide-PEG 5,000-peptide and 4-arm star [peptide-PEG 2,500]₄-C bioconjugates using percolation theory. Our study shows that the macroscopic gelation rates for these bioconjugates in NaCl are slower compared to the more chaotropic salts, NaBr and NaI.

Experimental

Materials and Methods

All peptide bioconjugate syntheses and purification protocols can be found in our previous work¹⁷. Briefly, peptides were synthesized using solid phase peptide synthesis. All PEG-peptide conjugation chemistry used standard Fmoc deprotection followed by the coupling of an asymmetric carboxylate functionalized PEG to the free amine of the peptide.

FTIR Spectroscopy

In this work, the characterization of peptide secondary structure was measured with a Nicolet i550 ATR-FTIR instrument with a KBr beamsplitter. Peptide solutions of 30.0 mg/ml were prepared in 3.5 M solutions of NaCl, NaBr or NaI. Determination of peptide secondary structure was measured at room temperature in the amide I region, 1610 to 1695 cm^{-1} wavenumber range²². Data was taken as an average of 128 scans at a resolution of 8 cm^{-1} and displayed as second-derivative spectra calculated using Savitzky-Golay algorithms²³.

Dynamic Light Scattering

Dynamic Light Scattering (DLS) measurements were used in order to characterize the rate of polymer cluster formation for peptide-PEG 5,000-peptide and [peptide-PEG 2,500]₄-C constructs in electrolyte solutions of 3.5M NaCl, NaBr or NaI. 1.0 mg/ml solutions of these peptide bioconjugates with each salt were placed in a 1.0 cm pathlength disposable cuvette. Polymer aggregate size measurements were recorded on a Malvern DLS every 4 minutes for 24 hours.

Microrheology

Passive microrheology was used to characterize the macroscopic mechanical properties for the peptide-PEG 5,000-peptide and [peptide-PEG 2,500]₄-C constructs exposed to each of the 3.5M salts. Fluorescent particles that were surface

functionalized with P108 pluronic²⁴ were added to polymer-peptide solutions such that 100 – 150 particles were simultaneously imaged using an oil immersion 63x inverted fluorescent microscope. Matlab algorithms^{25–27} were compiled and modified for random walk particle tracking on videos that were taken for 300 frames at a frame rate of 30Hz. The calculated time dependent particle average mean square displacement (MSD), $\langle \Delta r(\tau)^2 \rangle$, as it relates to intermolecular bioconjugate peptide self-assembly can be correlated with the Stokes-Einstein equation $\langle \Delta r(\tau)^2 \rangle = \langle |r(t+\tau) - r(t)|^2 \rangle = dkt\tau/3\pi\eta a$ to calculate viscoelastic properties as well as sol-gel transition kinetics, where d is the diffusion coefficient, kt is thermal energy, τ is the lag time, η is the viscosity and a is the probe particle size.

Results and discussion

The hydrating nature of kosmotropic ions typically lowers peptide solubility that increases intramolecular peptide interaction and stabilizes peptide secondary structure. In contrast, chaotropes typically increase peptide solubility by concentrating near poorly hydrating regions of the peptide²⁸. In our system, we would expect the build-up of chaotropic ions near the hydrophobic face to decrease helicity and increase solubility. The following results show that this classic trend is reversed.

From the results shown in Figure 1, peptide secondary structure correlates to a ‘reverse’ Hofmeister trend. ATR-FTIR spectroscopy of our peptide was conducted in the presence of sodium based Hofmeister anions (a) Cl⁻, (b) Br⁻, and (c) I⁻. In all cases, we observed that an increase in ion concentration promotes peptide charge-screening that correlates with a more pronounced signal 1650 cm^{-1} . This suggests an increased α -helical secondary structure with increased ion concentration. These findings are highlighted in the insets for figure 1 (a-c). A comparison of figures 1 (a-c) shows that the helical signature are more pronounced for the chaotropic ions. The shoulder at 1640 cm^{-1} is characteristic for the random coil, and this shoulder is present only in the teal spectrum at 0 M salt concentration. The shoulder vanishes with increasing salt concentration corroborating prior findings that peptide folding is driven by charge-screening. The peaks at 1630 cm^{-1} are artefacts of the lysine amino acid, arising from the lysine side chain amine (NH³⁺) bending^{22,29}.

The data in figure 1 (d) compares the effects of Hofmeister anions on peptide secondary structure. As the ions become increasingly chaotropic from Cl⁻ < Br⁻ < I⁻, the α -helical band at 1650 cm^{-1} becomes increasingly prevalent, suggesting a larger population of the α -helices in the chaotropic solutions. This is particularly evident for the iodide anion where the decrease in the band at 1675 cm^{-1} corresponds with a loss of β -sheet character. We believe that the localization of the increasingly chaotropic Br⁻ and I⁻ ions at the peptide’s hydrophobic face contributes to enhanced charge-screening resulting in an increase in the ensemble average helicity. Also, the mid-kosmotropic/chaotropic nature of the chloride anion does not

promote significant charge localization near the hydrophobic peptide face. As a result, the weakest FTIR signal at 1650 cm^{-1} is observed for the chloride ion.

Microrheology was used to examine the critical gelation transitional dynamics that result from the self-assembly of the peptide-PEG 5,000-peptide and [peptide-PEG 2,500]₄-C in the three salts, NaCl, NaBr and NaI at 3.5 M. Figure 2 shows a series of log-log plots for the average particle MSD as a function of lag time, τ . Diffusive behavior is observed for both linear- and star-peptide bioconjugates upon initial exposure to chloride, bromide or iodide ions as shown in figures 2 (a-f) where slopes equal to one demonstrates the viscous nature of the solution at early times³⁰.

Figure 2 (a) shows the peptide-PEG 5,000-peptide transition after 6 hours with measurements taken in 20-minute intervals. Likewise, figure 2 (b) shows a transition to the gel regime occurring after only 2 hours for the linear peptide bioconjugate in NaBr. The results in figure 2 (c) show a gel transition after 1 hour in NaI. The decreasing slope as a function of time highlights the increasingly subdiffusive nature of the linear bioconjugate as the polymer aggregates form a percolated network. The observed zero slope that is reached for each of the systems occurs at noticeably different rates but nonetheless reflects arrested particle motion that signals macroscopic gel-like elastic behavior³¹.

Figures 2 (d-f) show the ion effect of electrolytes on the percolating nature of the star-block [peptide-PEG 2,500]₄-C. These results are consistent with our previous findings, where the star bioconjugates show no time dependent changes in mechanical behavior¹⁷. Diffuse behavior was also observed for the star constructs in NaCl, NaBr and NaI, and the viscous nature persisted throughout a ten-day experimental period as confirmed by MSD slopes with $\theta=1$. These findings suggest that intramolecular self-assembled aggregation is dominant for the 4-arm structures that have minimal influence on material mechanical properties as opposed to the percolated intermolecular interactions observed in the peptide-polymer-peptide linear constructs.

Time-cure superposition was used to generate the pregel and postgel curves shown in Figure 3, constructed through 'a' horizontal time and 'b' vertical MSD shift factors of the data from figure 2. The initial MSD data for both peptide-PEG 5,000-peptide and [peptide-PEG 2,500]₄-C bioconjugates in both NaI and NaBr have a slope equal to $d\ln(\Delta r^2(\tau))/d\ln\tau = 1$ that defines the diffusive pregel with liquid mechanical properties. The superposition requires the MSD v. time data from each series to undergo a horizontal translation by multiplying the lag time data by a polymer relaxation time shift factor and a vertical translation by manipulation of the MSD data by a creep compliance multiplier. The horizontal and vertical shift factors for each of the curves from the data series in figure 3 were selected to position the subsequent MSD data curve over the prior curve to produce a best-fit line. The time-cure superposition for peptide-PEG 5,000-peptide is shown in figures 3 (a-c) for NaCl, NaBr and NaI salts. This results in the construction of pregel master curves until a discontinuity in the superposition is reached that highlights the sol-gel

transition region. The change in the macroscopic mechanical properties is an indication of the formation of the infinite percolation cluster. A postgel master curve is constructed in reverse for the MSD data after sol-gel transition region by the same method that leads to a pregel-postgel crossover. This methodology results in a quantitative measure of the critical gel time^{20,32}. Peptide-PEG 5,000-peptide in NaCl shows a pregel-postgel crossover after six hours while in NaBr the sol-gel transition occurs after two hours. For peptide-PEG 5,000-peptide in NaI, the sol-gel transition occurs after one hour.

A semi-logarithmic plot of the values for polymer relaxation time "a" and creep compliance "b" shift factors are shown in figure 4. The divergence of the data points for the horizontal and vertical shift factors yield a precise time for the dynamic sol-gel transition. Compared with the sol-gel transition data for NaCl that takes place after 6 hours, for the peptide-PEG 5,000-peptide bioconjugate in NaBr from figure 4 (a), the pregel and postgel shift factors diverge from a critical gel time of 155 minutes. A faster transition to the critical gel region is observed in figure 4 (b) for peptide-PEG 5,000-peptide in NaI of 75 minutes. The time scale for the formation of incipient gels is consistent with our previous findings from NaCl with a sol-gel transition time at 386 minutes, but the trend in these findings are not in agreement with the typical principles of the Hofmeister series. We observe that increased ion chaotropic nature leads to increased peptide folding. Furthermore, we do not observe any divergence for [peptide-PEG 2,500]₄-C with any of the anions tested. This suggests that the inter- and intra-molecular self-assembly behavior dominates over the specific ion effects to control the thermodynamics of the gel regime, but the specific ion interactions dictate the kinetics of gelation.

Dynamic light scattering measurements were used to observe self-assembly of the discrete growing clusters as a function of time. The change in cluster sizes for peptide-PEG 5,000-peptide and [peptide-PEG 2,500]₄-C bioconjugates were determined in NaBr and NaI and compared with cluster sizes formed in NaCl. These findings are shown in figure 5, and the cluster size formation rates correlate well with our results from microrheology. For the peptide-PEG 5,000-peptide bioconjugate, larger clusters were formed more rapidly in the presence of bromide and iodide anions when compared to the clusters formed in the presence of chloride anions. This finding corroborates the kinetic studies accomplished with microrheology, where faster forming clusters will lead to a faster sol-gel transition into the elastic regime. Additionally, the bioconjugated [peptide-PEG 2,500]₄-C structure with bromide and iodide formed larger clusters compared to the clusters formed in sodium chloride, but the sizes of these clusters quickly plateaued before the reaching the percolation threshold.

The faster rates of observed self-assembly for peptide-PEG 5,000-peptide in systems that become increasingly chaotropic is contrary to the traditional view for Hofmeister ion interactions with peptides as discussed earlier. Deyerle et al. studied anion Hofmeister effects on the phase transition temperatures of L44 pluronic copolymers. Weakly hydrating

chaotropic anions that include Γ^- and SCN^- anions were shown to have a tendency toward the hydrophobic PPO solute/aqueous interface. These ions decrease the interfacial tension at the interface to make the PPO more soluble. In turn, the chaotropic anions increase the phase transition temperature of the pluronic. Mid-kosmotropic/chaotropic ions that include Br^- , Cl^- , and NO_3^- were shown to increase surface tension yielding the opposite effect on the phase transition temperature. The effects of strongly hydrating kosmotropic ions results in a decreased the phase transition temperature of the L44 pluronic, but the mechanism for this phenomenon was shown to be the dehydration of the hydrophilic PEG groups that also lower the polymer's solubility. These well hydrating ions interact with the water molecules around the hydrophilic PEG moieties to lower the entropy of hydration making them less available to the polymer³³.

Similar reasoning behind findings from Cho et al. show "salting-out" behavior for kosmotropic ions that decrease the lower critical solution temperature (LCST) for elastin, while chaotropic ions had a "salting-in" effect that increased the LCST³⁴. Near the hydrophobic regions, self-associated water networks that create the polymer/water interfacial tension result in cavities that can lead to high local concentrations of the poorly hydrating chaotropes¹³. The accumulation of chaotropic ions in the proximity of the hydrophobic face of our peptide can lead to the increase in secondary structure shown in figure 1, which, in turn, can lead to increased self-assembly rates. Our prior studies have shown that these rationally designed linear peptide bioconjugate fold into an α -helical secondary structure as a consequence of the intramolecular screening of the positive charges^{17,19} from the lysine groups at position 8, 9 and 12 of the peptide sequence. Others have investigated the consistency of the Hofmeister series, questioning the generality of the well-established ion sequence³⁵. Notably, a 'reverse' Hofmeister effects has been observed for cationic proteins³⁶ and hydrophobic systems³⁷, which is the case for our peptide with a net +3 charge and a hydrophobic face.

Figure 6 shows how the measurement of the sol-gel transition time was determined for the peptide-PEG 5,000-peptide bioconjugate in NaBr and NaI. The formation of an intermolecular percolated network requires the self-assembly of 'crosslinking' polymers that occurs through the random molecular associations to initially form small networks. As a critical probability is reached where $p \sim p_c$ the formation of an insoluble infinite percolated cluster develops that swells the matrix and results in a material with elastic properties. Near this critical region, the polymer's longest relaxation time ' τ_L ' and creep compliance ' J_e^0 ' follow a power law divergence behavior proportional to the values obtained for the 'a' and 'b' superposition shift factors. Percolation theory makes the scaling near the transition region $a \sim \tau_L \sim \varepsilon^y = ((|t-t_c|)/t_c)^y \sim ((|p-p_c|)/p_c)^y$ and $b \sim 1/J_e^0 \sim \varepsilon^z = ((|t-t_c|)/t_c)^z \sim ((|p-p_c|)/p_c)^z$. 'y' and 'z' are both critical scaling exponents, where 'y' is the longest relaxation time exponent and 'z' is the creep compliance exponent. Both exponents use ' t_c ' as the critical

gel time, and ' ε ' = $((|t-t_c|)/t_c) = ((|p-p_c|)/p_c)$ is the distance away from the critical gel region^{20,38,39}.

For peptide-PEG 5,000-peptide in NaBr shown in figures 6 (a) & 6 (b), a sweep of critical gel times in the pregel and postgel regions result in a critical gel time ' t_c ' equal to 155 minutes. Before the gel point, the dynamic scaling exponents for the pregel are determined as the slopes with $y = 3.65$ and $z = 1.91$. For the postgel region in figure 6 (b), NaBr ions result in $y = 5.43$ and $z = 2.70$. For the iodide system in figures 6 (c) and 6 (d), a critical gel time of 75 minutes was obtained, and pregel values were found to be $y=4.31$ and $z=3.17$. In the postgel region, NaI resulted in $y = 4.02$ and $z = 2.67$.

Calculation of the viscoelastic critical relaxation exponent 'n' is the ratio of 'z' and 'y'²⁰. For NaBr, the viscoelastic exponent is equal to 0.51, which can be interpreted as a polymeric self-assembly that follow a Zimm model for a percolation cluster network that is held together by densely cross-linked, highly entangled polymers³⁸. As the system becomes increasingly chaotropic in an environment surrounded by ions of sodium iodide, we determine a different set of a dynamics with viscoelastic exponent of 0.70, which can be interpreted as a Rouse chain. The Rouse chain resembles a ball and chain that is connected intermolecularly at junction points⁴⁰.

ATR-FTIR results show that exposure to an increasingly chaotropic environment enhances ensemble average peptide folding for our coiled-coil forming peptides. The formation of tetrameric helical bundles maximizes the burial of hydrophobic side groups^{16,19}. These findings correspond well with our results using microrheology and DLS that confirm larger clusters formed at a faster rate with chaotropic anions. A hierarchical relationship exists between the folded orientation and the cluster size as seen using DLS^{41,42}. In this system, the self-assembly is a consequence of the formation of amphiphilic helices. The increase in the population of helical bundles should lead to a more Rouse-like structure, where peptide crosslinks dominate over the entanglement of the PEG-block.

Ion	Sol-gel transition time t_c	Viscoelastic exponent n
Chloride ¹⁷	386 minutes	0.33 ± 0.05
Bromide	155 minutes	0.51 ± 0.03
Iodide	75 minutes	0.70 ± 0.03

Table 1. Viscoelastic parameters and sol-gel transition rates for 3mM peptide-PEG 5,000-peptide triblock conjugates obtained from microrheology for 3.5M sodium-based ion solutions.

Table 1 shows the results for Cl^- , Br^- and Γ^- . The table highlights that our linear peptide bioconjugates show increasingly Rouse-like behavior with increasingly chaotropic anions. Further evidence from DLS results support this finding, where the size of detectable polymer clusters increases with ions that are more chaotropic. The formation of larger clusters was also consistent with the [peptide-PEG 2,500]₄-C peptide

bioconjugates that did not self-assemble to form gels. Furthermore, the larger percolated cluster sizes in the presence of chaotropic ions is consistent with the 'reverse' Hofmeister mechanism, where the evolution of self-assemblies is driven by locally high concentrations of chaotropic ions near the hydrophobic helical face, yielding Rouse-like behavior for a loosely connected network held together at coiled-coil peptide 'junction points'. In systems with less chaotropic anions, we observed smaller polymer clusters and smaller values for the viscoelastic exponent, suggesting that macroscale elasticity is a consequence of random entanglement⁴³.

Conclusions

In this work, we demonstrate how anions in the Hofmeister series can influence the kinetics of gelation. We found a 'reverse' Hofmeister trend where increasingly chaotropic ions result in enhanced helical folding, faster sol-gel kinetics and higher viscoelastic exponents. We believe the mechanism stems from the poorly hydrating ions lowering the peptide/water interfacial tension near the peptide's hydrophobic face. The local ion concentration produces an enhanced charge screening effect, which increases the ensemble average helical conformation. As a result, the self-assembly of coiled-coils with more chaotropic anions yields higher viscoelastic exponents. In our bioconjugate system, the combination of hydrophobic- and charge-screening interactions leads to faster gelation kinetics and more Rouse-like behavior. This work provides new experimental evidence of a 'reversed' Hofmeister series.

Conflicts of interest

There are no conflicts to declare.

Acknowledgements

We gratefully acknowledge financial support from the National Institutes of Health/National Institute of General Medical Sciences (NIH-NIGMS) award [R25GM056833] and NSF CREST Center for Interface Design and Engineered Assembly of Low Dimensional systems (IDEALS), NSF grant number HRD-1547830. RT also acknowledges partial funding from AFOSR [FA9550-14-1-0263] and NSF-CBET award [1506539]. We would like to thank Kelly Schultz for microrheology insight as well as Matthew Kubilius for assistance with MALDI-MS characterization.

Notes and references

- 1 D. R. Hathaway and R. S. Adelstein, *Proc. Natl. Acad. Sci.*, 1979, **76**, 1653–1657.
- 2 E. Behrmann, M. Müller, P. A. Penczek, H. G. Mannherz, D. J. Manstein and S. Raunser, *Cell*, 2012, **150**, 327–338.
- 3 H. Hidaka, T. Yamaki, T. Totsuka and M. Asano, *Mol.*

- 4 *Pharmacol.*, 1979, **15**, 49–59.
- 5 P. H. von Hippel and T. Schleich, *Acc. Chem. Res.*, 1969, **2**, 257–265.
- 6 P. H. von Hippel and K.-Y. Wong, *Biochemistry*, 1963, **2**, 1387–1398.
- 7 M. G. Cacace, E. M. Landau and J. J. Ramsden, *Q. Rev. Biophys.*, 1997, **3**, 241–277.
- 8 K. D. Collins, *Methods*, 2004, **34**, 300–311.
- 9 Y. Zhang and P. S. Cremer, *Curr. Opin. Chem. Biol.*, 2006, **10**, 658–663.
- 10 A. H. Crevenna, N. Naredi-Rainer, D. C. Lamb, R. Wedlich-Söldner and J. Dzubiella, *Biophys. J.*, 2012, **102**, 907–915.
- 11 W. D. Kohn, C. M. Kay and R. S. Hodges, *J. Mol. Biol.*, 1997, **267**, 1039–1052.
- 12 T. E. Creighton, *Proteins: structures and molecular properties*, Macmillan, 1993.
- 13 M. Ries-Kautt and A. Ducruix, in *Methods in enzymology*, Elsevier, 1997, vol. 276, pp. 23–59.
- 14 Y. Zhang and P. S. Cremer, *Annu. Rev. Phys. Chem.*, 2010, **61**, 63–83.
- 15 H. X. Zhou, *Proteins Struct. Funct. Genet.*, 2005, **61**, 69–78.
- 16 K. a. Dill and T. M. Truskett, *Annu. Rev. Biophys. Biomol. Struct.*, 2005, **34**, 173–199.
- 17 V. Jain, A. Jimenez, C. Maldarelli and R. S. Tu, *Langmuir*, 2008, **24**, 9923–9928.
- 18 S. C. O'Neill, Z. H. Bhuiyan and R. S. Tu, *Soft Matter*, 2017, **13**, 7521–7528.
- 19 V. P. Jain, C. Maldarelli and R. S. Tu, *J. Colloid Interface Sci.*, 2009, **331**, 364–370.
- 20 V. P. Jain and R. S. Tu, *Int. J. Mol. Sci.*, 2011, **12**, 1431–1450.
- 21 T. H. Larsen and E. M. Furst, *Phys. Rev. Lett.*, 2008, **100**, 1–4.
- 22 K. M. Schultz and E. M. Furst, *Soft Matter*, 2012, **8**, 6198–6205.
- 23 B. H. Stuart and D. J. Ando, *Biological applications of infrared spectroscopy*, John Wiley & Sons, 1997.
- 24 A. Savitzky and M. J. E. Golay, *Anal. Chem.*, 1964, **36**, 1627–1639.
- 25 A. J. Kim, V. N. Manoharan and J. C. Crocker, *J. Am. Chem. Soc.*, 2005, **127**, 1592–1593.
- 26 E. R. Dufresne, T. M. Squires, M. P. Brenner and D. G. Grier, *Phys. Rev. Lett.*, 2000, **85**, 3317–3320.
- 27 V. Pelletier, N. Gal, P. Fournier and M. L. Kilfoil, *Phys. Rev. Lett.*, 2009, **102**, 100–103.
- 28 S. Sathaye, A. Mbi, C. Sonmez, Y. Chen, D. L. Blair, J. P. Schneider and D. J. Pochan, *Wiley Interdiscip. Rev. Nanomedicine Nanobiotechnology*, 2015, **7**, 34–68.
- 29 M. Jaspers, A. E. Rowan and P. H. J. Kouwer, *Adv. Funct. Mater.*, 2015, **25**, 6503–6510.
- 30 B. H. Stuart, *Infrared Spectrosc. Fundam. Appl.*, 2005, 1–224.
- 31 C. Veerman, K. Rajagopal, C. S. Palla, D. J. Pochan, J. P. Schneider and E. M. Furst, *Macromolecules*, 2006, **39**, 6608–6614.
- 32 V. Breedveld and D. J. Pine, *J. Mater. Sci.*, 2003, **38**, 4461–4470.
- 33 K. M. Schultz and E. M. Furst, *Lab Chip*, 2011, **11**, 3802.

ARTICLE

PCCP

- 33 B. A. Deyerle and Y. Zhang, *Langmuir*, 2011, **27**, 9203–9210.
- 34 Y. Cho, Y. Zhang, T. Christensen, L. B. Sagle, A. Chilkoti and P. S. Cremer, *J. Phys. Chem. B*, 2008, **112**, 13765–13771.
- 35 N. Schwierz, D. Horinek, U. Sivan and R. R. Netz, *Curr. Opin. Colloid Interface Sci.*, 2016, **23**, 10–18.
- 36 Y. Zhang and P. S. Cremer, *Proc. Natl. Acad. Sci.*, 2009, **106**, 15249–15253.
- 37 T. López-León, M. J. Santander-Ortega, J. L. Ortega-Vinuesa and D. Bastos-González, *J. Phys. Chem. C*, 2008, **112**, 16060–16069.
- 38 J. E. Martin, D. Adolf and J. P. Wilcoxon, *Phys. Rev. A*, 1989, **39**, 1325–1332.
- 39 J. E. Martin, D. Adolf and J. P. Wilcoxon, *Phys. Rev. Lett.*, 1988, **61**, 2620–2623.
- 40 B. H. Zimm, *J. Chem. Phys.*, 1956, **24**, 269–278.
- 41 K. L. Wooley, J. S. Moore, C. Wu and Y. Yang, *Proc. Natl. Acad. Sci.*, 2000, **97**, 11147–11148.
- 42 R. S. Tu and M. Tirrell, *Adv. Drug Deliv. Rev.*, 2004, **56**, 1537–1563.
- 43 A. E. Likhtman and T. C. B. Mcleish, 2002, 6332–6343.

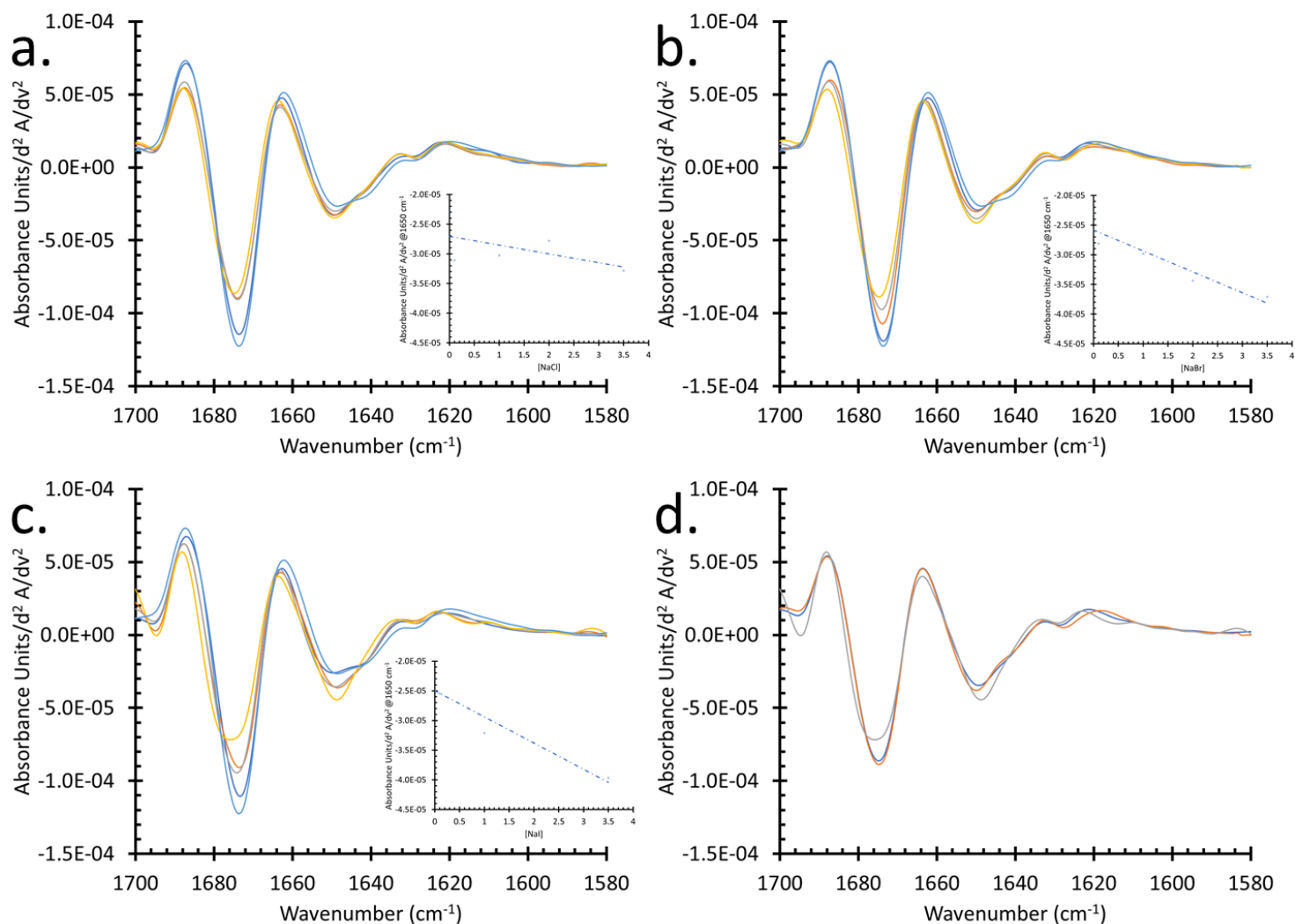


Figure 1. Second derivative peptide ATR-FTIR spectra for the amide I region as a function of salt concentration. (a) NaCl (b) NaBr (c) NaI. In all cases, teal, blue, orange, grey and yellow are increasing in ion concentration from 0 M, 0.1 M, 1.0 M, 2.0 M and 3.5 M. Insets for each figure show ion concentration effects on the intensity of the spectra at 1650 cm⁻¹ (d) A comparison of Hofmeister salts at 3.5 M, NaCl (blue), NaBr (orange) and NaI (grey).

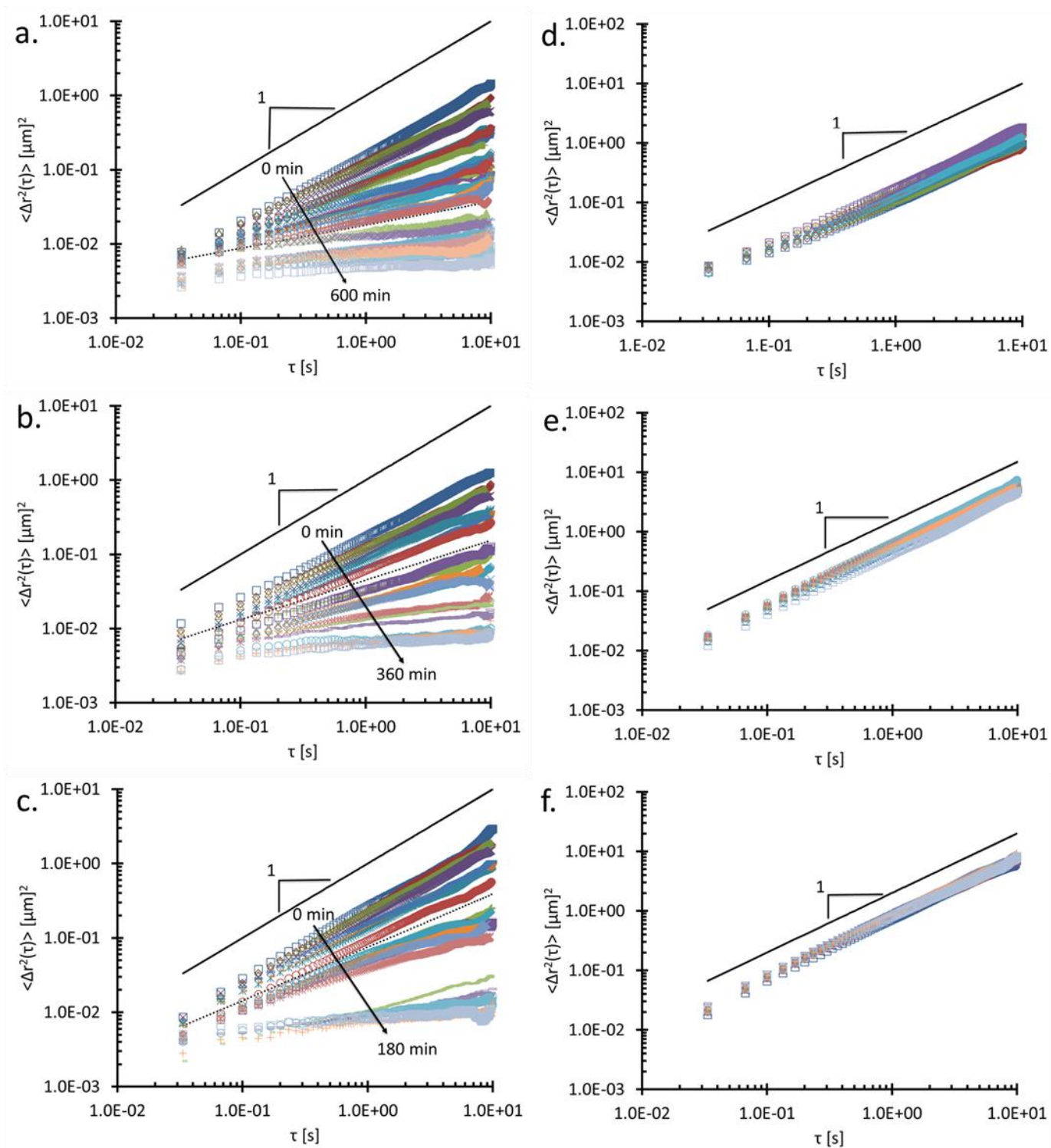


Figure 2. Particle MSD is plotted as a function of time for peptide-PEG-5,000-peptide in figure 2 (a-c) and [peptide-PEG 2,500]₄-C figure 2 (d-f) in increasingly chaotropic salts NaCl figure 2 (a & d) NaBr figure 2 (b & e) and NaI figure 2 (c & f). The individual curves represent the measured MSD and the monitored gelation process as a function of time on a log-log plot.

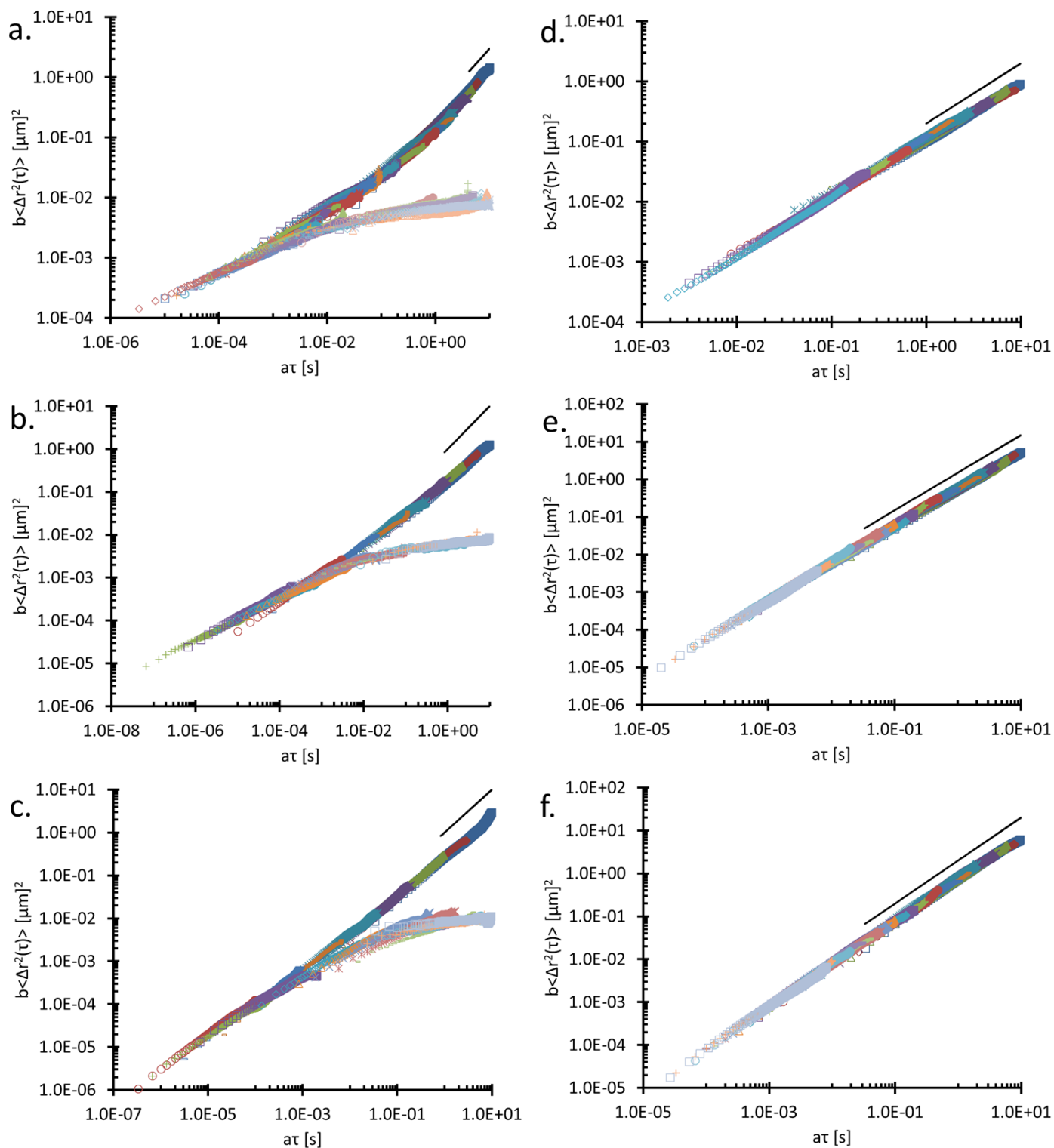


Figure 3. MSD superposition corresponding to increasingly chaotropic ions for linear peptide constructs figure 3 (a-c) and 4-arm peptide constructs figure 3 (d-f). Starting with the initial diffusive MSD data, subsequent curves are shifted by shift factors 'a' and 'b' horizontally [$a\tau$] and vertically [$b \langle \Delta r^2(\tau) \rangle$] that demonstrate changes in viscoelastic properties.

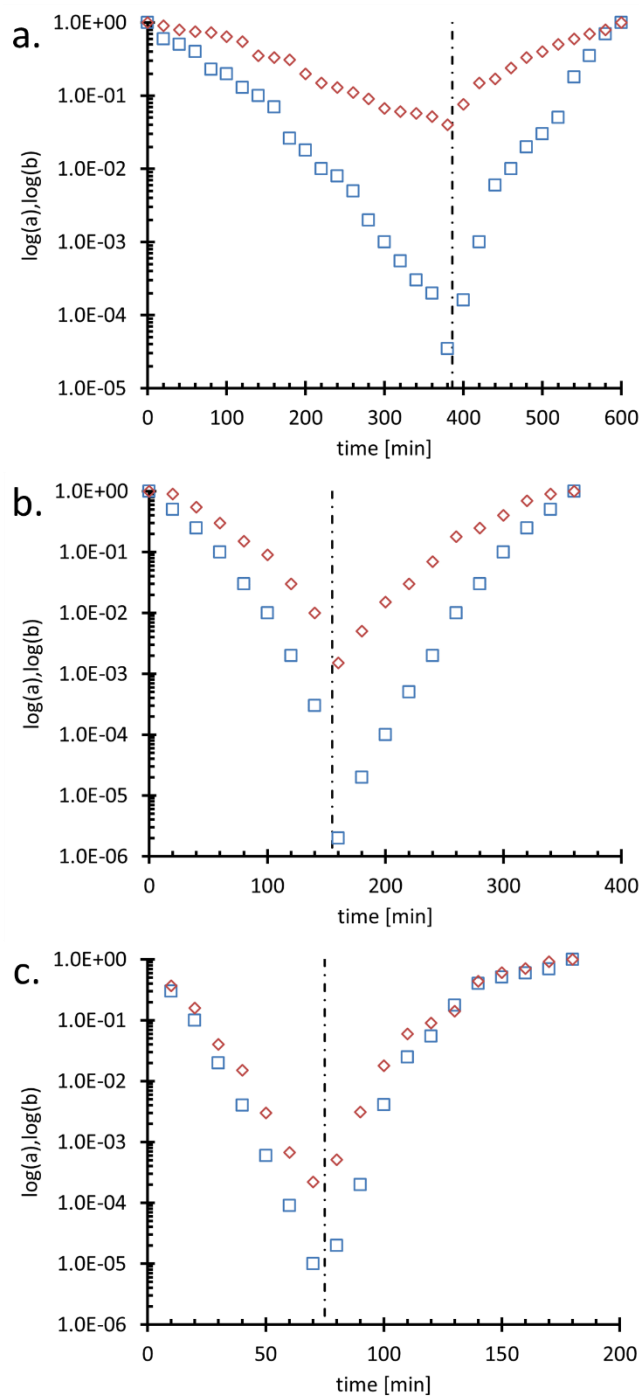


Figure 4. Shifts for peptide-PEG 5,000-peptide in NaCl (a), NaBr (b) and NaI (c) are shown. Blue squares are the time 'a' shift factor and red diamonds are the MSD 'b' shift factor. The critical gel point is determined by the divergence of the shift factors.

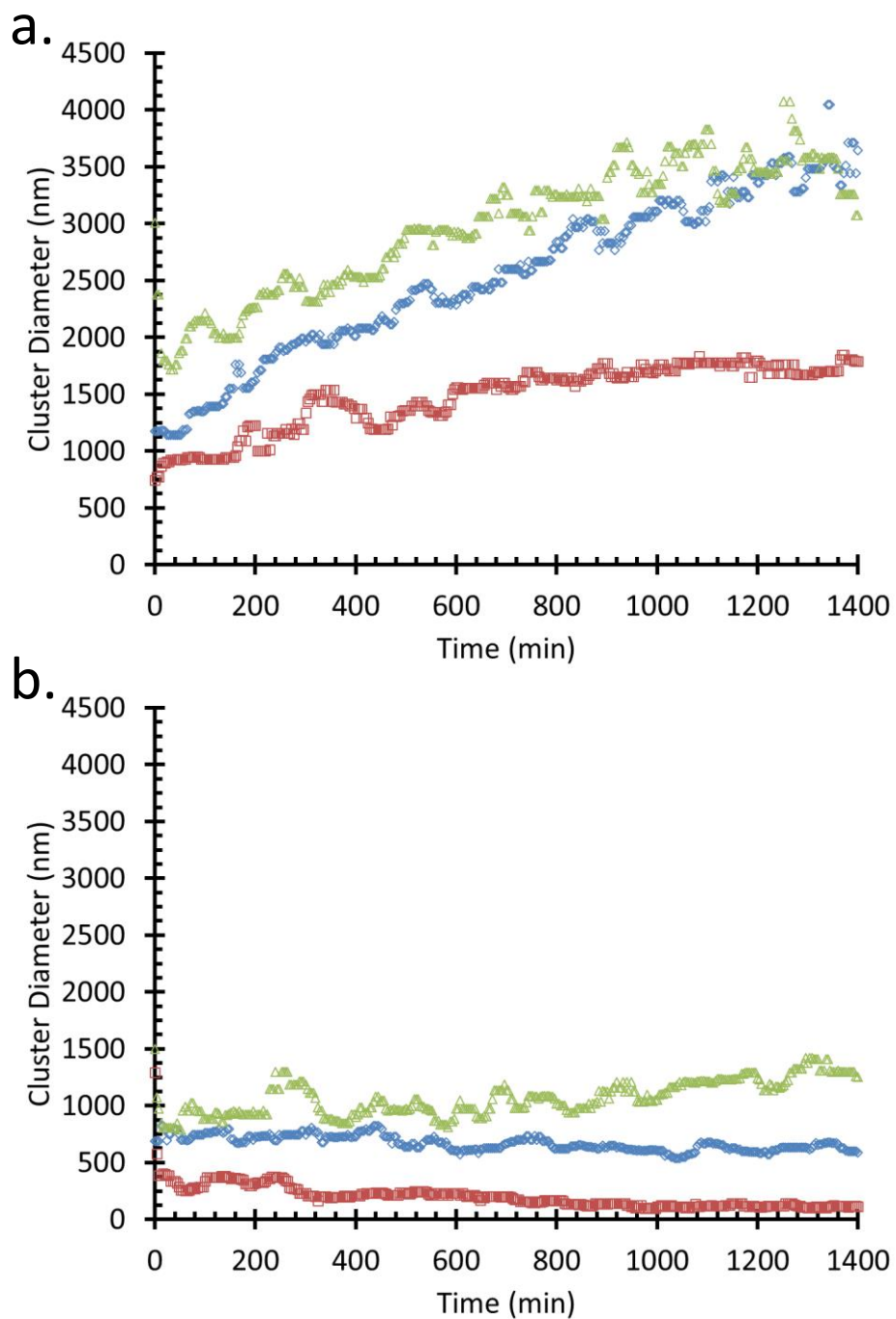


Figure 5. Dynamic light scattering plots for the rate of percolation cluster formation as a function of the Hofmeister series. (a) Aggregate size for peptide-PEG 5,000-peptide in NaCl (red) NaBr (blue) and NaI (green) and (b) Aggregate size for [peptide-PEG 2,500]₄-C.

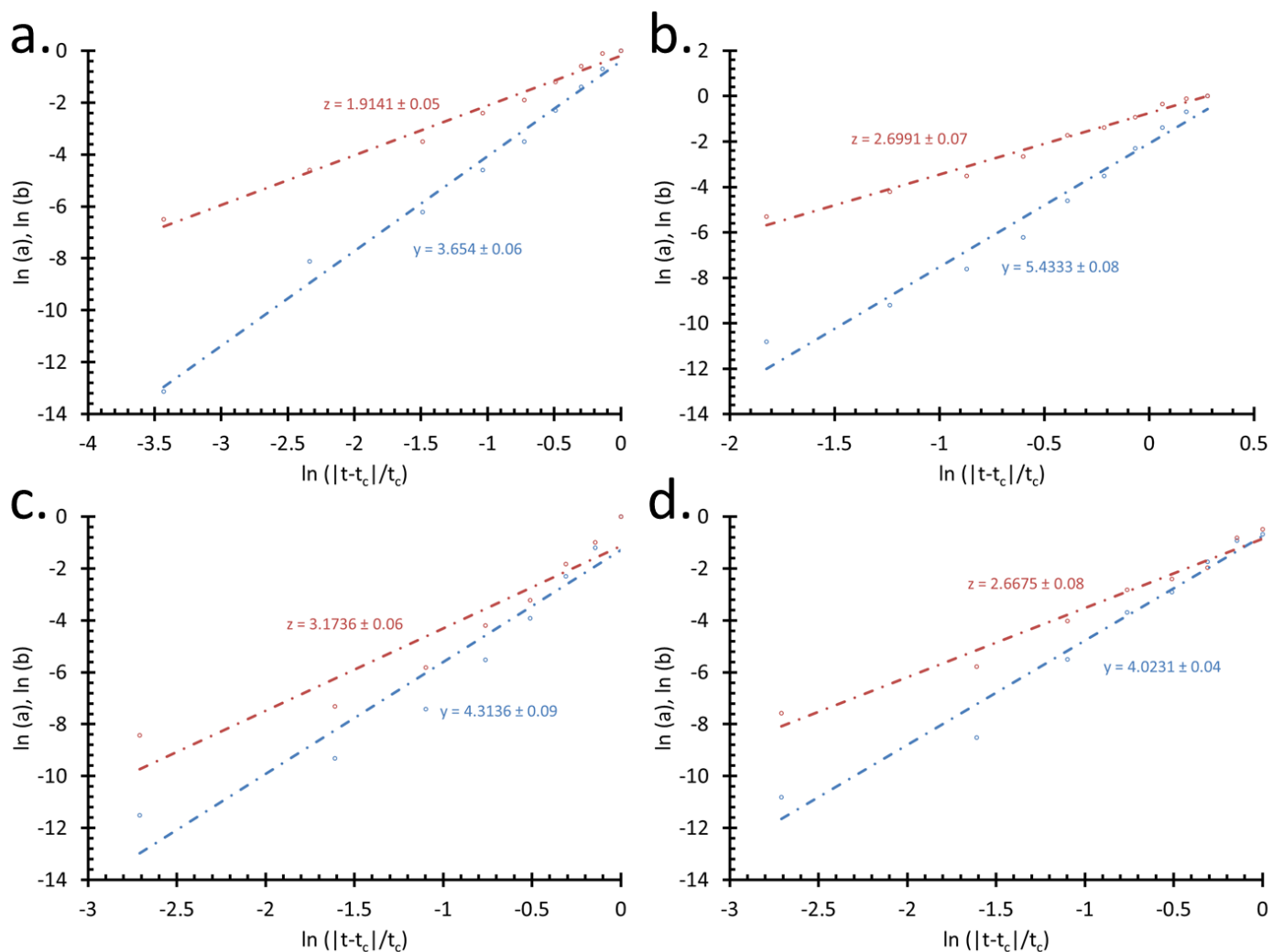
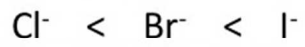


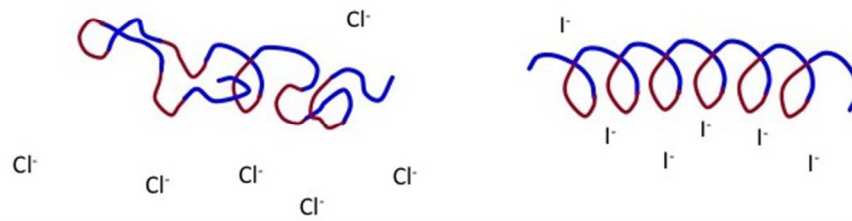
Figure 6. Peptide PEG 5,000-peptide conjugate relaxation time in blue and MSD in red factors are plotted against the distance from the critical gel point for fitting to determine the critical scaling exponents and the critical relaxation exponent for (a) NaBr pregel (b) NaBr postgel (c) NaI pregel and (d) NaI postgel.

'Reverse' Hofmeister Series



Kosmotropes

Chaotropes



246x102mm (72 x 72 DPI)